

A&A manuscript no.
(will be inserted by hand later)
Your thesaurus codes are:
12(11.03.5; 11.04.1; 11.05.1; 11.11.1 - 12.03.3)

**ASTRONOMY
AND
ASTROPHYSICS**
November 4, 2018

Dynamics of the X-ray clusters Abell 222, Abell 223 and Abell 520 *

D. Proust¹, H. Cuevas², H.V. Capelato³, L. Sodré Jr.², B. Tomé Lehodey³, O. Le Fèvre⁴, and A. Mazure⁴

¹ DAEC, CNRS, Observatoire de Paris-Meudon, 92195 Meudon Cedex, France.

² Departamento de Astronomia IAG/USP, Av. Miguel Stefano 4200, 04301-904, São Paulo, Brazil

³ Divisão de Astrofísica INPE/MCT, 12225-010, São José dos Campos, Brazil

⁴ Laboratoire d'Astronomie Spatiale, Les Trois Lacs, 13012 Marseille, France

Received date; accepted date

Abstract. We present the results of a dynamical analysis of three rich, X-ray luminous galaxy clusters, Abell 222, Abell 223 and Abell 520, that are at intermediate redshifts. Our study is based on radial velocities for 71 cluster members, respectively 30 for A222, 20 for A223 and 21 for A520, measured from spectra obtained at the Canada-France-Hawaii Telescope, the European Southern Observatory, and the Pic du Midi Observatory, and supplemented with radial velocities from the literature. A222 galaxies have slightly higher velocities than those of A223, with bi-weighted mean velocity of $V_{bi} = 64242 \pm 194 \text{ km s}^{-1}$ for A222, and of $V_{bi} = 63197 \pm 266 \text{ km s}^{-1}$ for A223. The velocity dispersions of the two clusters are about the same: $\sigma_{bi} = 1013 \pm 150 \text{ km s}^{-1}$ and $\sigma_{bi} = 1058 \pm 160 \text{ km s}^{-1}$ for A222 and A223, respectively. For A520 we obtain $V_{bi} = 60127 \pm 284 \text{ km s}^{-1}$ with $\sigma_{bi} = 1250 \pm 189 \text{ km s}^{-1}$. We also give mass and mass-luminosities ratio estimates for each cluster separately. We argue that these clusters are presently undergoing strong dynamical evolution and that A222 and A223 will probably merge in the future. We have applied a Principal Component Analysis to a sample of 51 CFHT spectra to produce a spectral classification for these galaxies. This classification has allowed us to show that the morphological and kinematical segregations were already established in these intermediate redshift clusters.

Key words: Galaxies: redshifts of – clusters of – sub-clustering; Cosmology

1. Introduction

Clusters of galaxies are the largest gravitationally bound systems, with the following components contributing to

Send offprint requests to: D. Proust

* based on observations made at ESO-La Silla (Chile), at the Canada France Hawaii Telescope and at the Pic du Midi Observatory (France).

their total mass: dark matter, which is the dominant component, the hot X-ray emitting gas, that is the dominant baryonic component, and the stars and gas in galaxies. A valuable approach to determine the distribution of these components is offered by studying the relation between the global cluster properties which can be directly measured, such as the velocity dispersion σ , the total luminosity L , effective radii R_e , and morphological type distribution. Correlations between these intrinsic parameters have been found for many galaxy clusters, e.g. between richness and velocity dispersion (Danese, de Zotti & di Tullio 1980, Cole 1989), and between radius and luminosity (West, Oemler & Deckel 1989). Evidence pointing towards a close link between morphology and environment are the morphological segregation (Dressler 1980) and the correlation between type and velocity dispersion (Sodré et al. 1989), which we call kinematical segregation. Knowing whether these phenomena are due to initial conditions, environmental effects or both is one of the main questions to be answered in the study of these structures.

Morphological types, however, can be expensive to obtain. An interesting alternative is to use spectral classification to obtain spectral types (Sodré & Cuevas 1994, 1997; Folkes, Lahav & Maddox 1996). This procedure is based on a principal component analysis (PCA) of the spectra and allows to define a spectral classification that presents some advantages over the usual morphological classification: it provides quantitative, continuous and well defined types, avoiding the ambiguities of the intrinsically more qualitative and subjective morphological classification. This method has also been applied to the study of the ESO-Sculptor Survey (Galaz & de Lapparent 1998) and to the Las Campanas Redshift Survey (Bromley et al. 1998), and it was found that PCA allows to classify galaxies in an ordered and continuous spectral sequence, which is strongly correlated with the morphological type.

In this paper we present an analysis of three medium distant X-ray clusters, A222, A223 and A520, all of them belonging to the Butcher, Oemler & Wells (1983, hereafter

BOW83) photometric sample. For these clusters, very few redshifts exist, as found in the NED database¹. We have obtained new spectra which have enabled us to perform a preliminary study of their dynamical properties. The projected galactic densities of the clusters were compared to the X-ray emission images in order to seek for substructures inside these systems. From the observed spectra we have proceeded the spectral classification of the galaxies, allowing, for the first time, to study the morphological and kinematical segregations present in these clusters. In Section 2 we describe the observations, instrumentation, data reduction techniques and comparisons with previous measurements. In Section 3, the spatial distribution and kinematical properties are performed and discussed as well as mass and mass-luminosities ratio estimates. In Section 4 we analyze the spectral classification of the galaxies. Section 5 discuss the morphological and kinematical segregations. Finally, in Section 6 we present a summary of our main results.

2. Observations and Data Reductions

The analysis of the dynamical state of the clusters discussed here is based on a large set of velocities for the cluster galaxies. Multi-object spectroscopy has been performed at CFHT in November 1993 and at the ESO 3.60m telescope in December 1995. The instrumentation used at CFHT was the Multi Object Spectrograph (MOS) using the grism O300 with a dispersion of 240 Å/mm and the STIS CCD of 2048x2048 pixels of 21 μ m, leading to a dispersion of 5 Å/pixel. The instrumentation used at ESO was the ESO Faint Object Spectrograph and Camera (EFOSC) with the grism O300 yielding a dispersion of 230Å/mm and the TEK512 CCD chip of 512x512 pixels of 27 μ m giving a resulting dispersion of 6.3 Å/pixel. We completed the observations during an observing run at the 2.0m Bernard Lyot telescope at Pic du Midi observatory in January 1997, using the ISARD spectrograph in its long-slit mode with a dispersion of 233 Å/mm and with the TEK chip of 1024x1024 pixels of 25 μ m, corresponding to 5.8 Å/pixel. Typically, two exposures of 2700s each were taken for fields across the cluster. Wavelength calibration was done using arc lamps before each exposure (Helium-Argon at CFHT, Helium-Neon at ESO and Mercury-Neon at Pic du Midi lamps).

The data reduction was carried out with IRAF² using the MULTIRED package (Le Fèvre *et al.* 1995). The sky

¹ The NASA/IPAC Extragalactic Database (NED) is operated by the Jet Propulsion Laboratory, California Institute of Technology, under contract with the National Aeronautics and Space Administration

² IRAF is distributed by the National Optical Astronomy Observatories, which are operated by the Association of Universities for Research in Astronomy, Inc., under cooperative agreement with the National Science Foundation.

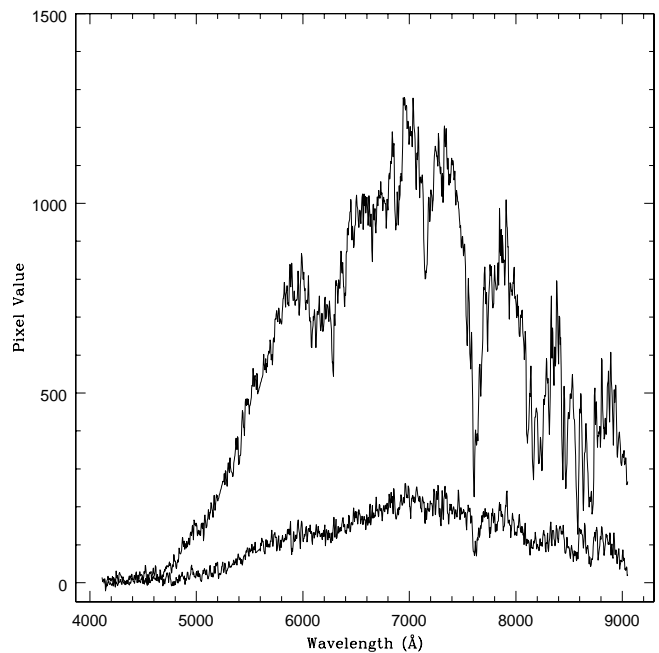


Fig. 1. Examples of two CFHT spectra of A222: one of a bright galaxy ($f_{57} = 17.87$) with a high signal-to-noise ratio ($R=6.59$) and the other of a fainter galaxy ($f_{57} = 18.98$) with low signal-to-noise ratio ($R=3.96$).

spectrum has been removed from the data in each slit by using measurements at each side of the galaxy spectra.

Radial velocities have been determined using the cross-correlation technique (Tonry and Davis 1979) implemented in the RVSAO package (Kurtz *et al.* 1991, Mink & Wyatt 1995) with radial velocity standards obtained from observations of late-type stars and previously well-studied galaxies.

From the total set of data we have retained 78 successful spectra of objects (28 for A222, 25 for A223 and 25 for A520) with a signal-to-noise ratio high enough to derive the measurement of the radial velocity with good confidence, as indicated in Table 1 by the R value of Tonry and Davis (1979). Note that since the templates used in the reduction were the same for all spectra, the R values contained in Table 1 are proportional to the signal-to-noise ratio of the spectra. Star contamination was very low (only 1 of the selected targets turned out to be a star). To help the reader to appreciate the kind of data discussed in this paper, we present in Figure 1 two spectra, one with high signal-to-noise ratio ($R=6.59$) and the other with low signal-to-noise ratio ($R=3.96$).

Table 1 lists positions and heliocentric velocities for the 78 individual galaxies in the clusters. For each galaxy we give also f and j band photometry from BOW83. The table is completed with a few galaxies observed by Newberry, Kirshner & Boroson (1988) and Sandage, Kristian & Westphal (1976). The table entries are:

1. galaxy number

2. right ascension (hour, min, sec)
3. declination (degree, minute, second)
4. f_{57} magnitude from Butcher *et al.* (1983).
5. $j - f_{57}$ color from Butcher *et al.* (1983).
6. heliocentric radial velocity with its error in km s^{-1}
7. R-value derived from Tonry & Davis (1979).
8. instrumentation and notes, **c**: 3.60m CFHT telescope, **e**: 3.60m ESO telescope, **I**: Newberry, Kirshner & Boroson (1988), **p**: 2.0m BL telescope, **s**: Sandage, Kristian & Westphal (1976).

In order to test the external accuracy of our velocities, we compared our redshift determinations (V_P) with data available in literature (V_L) for 5 galaxies observed in common (4 from Newberry, Kirshner & Boroson 1988, and 1 from Sandage, Kristian and Westphal 1976). The mean value of $(V_P - V_L)$ is very small, 27 km s^{-1} , and the null hypothesis that these two sets have the same variance but significantly different means can be rejected at the 99% level.

3. Spatial distribution and kinematical properties

3.1. The binary cluster A222 + A223

As already noticed by Sandage, Kristian & Westphal (1976), these two neighboring clusters have nearly the same redshift and probably constitute an interacting system which is going to merge in the future. Both are dominated by a particularly bright cD galaxy. They have a richness class R=3 and are X-ray luminous with $L_X(7 \text{ keV}) = 3.7 \pm 0.7 \cdot 10^{44} \text{ erg s}^{-1}$ and $1.5 \pm 0.6 \cdot 10^{44} \text{ erg s}^{-1}$ for A222 and A223, respectively (Lea and Henry, 1988). The BOW83 sample covers only the central regions of these two clusters and, in order to study the galaxy distribution in these systems, as well as to estimate the projected density for the galaxies in our sample (see below), we have built a more extensive, although shallower, galaxy catalog, covering a region of $45' \times 45'$ centered on the median position of the two clusters. This catalogue, with 356 objects, was extracted from Digital Sky Survey (DSS) images, using the software SExtractor (Bertin & Arnouts 1996). It is more than 90% complete to BOW83 magnitudes $f_{57} \sim 19$.

Figure 2 displays the significance map for the projected densities of galaxies in the region (cf. Biviano et al. 1996 for details on this type of map), as derived from the DSS sample. The overall distribution of galaxies is elongated along the direction defined by the two main clusters, showing extension from both sides and suggesting that both clusters belong to the same – probably still collapsing – structure.

In Figures 3a and 3b we display the isophotes of a wavelet reconstruction (Ru   & Bijaoui, 1997) of a ROSAT HRI X-ray image, superposed on the significance maps of the projected density of galaxies (dashed lines). In contrast with Figure 2 above, these maps were constructed

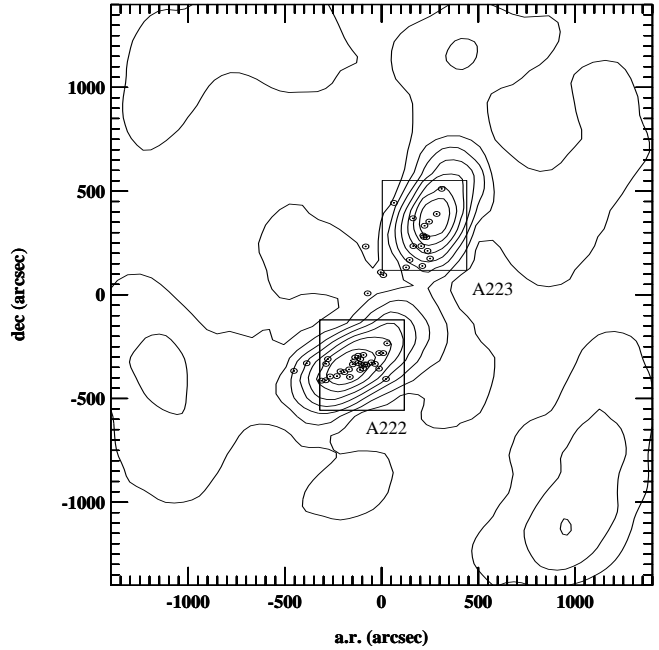


Fig. 2. Projected density map of the galaxies in the field of A222 and A223 (centered at $\alpha_{2000} = 01^h37^m41^s$, $\delta_{2000} = -12^\circ53'50''$). The galaxies were extracted from DSS images with the software SExtractor (see text). The circles with dots correspond to galaxies with measured radial velocities and belonging to the cluster. The squares display the areas covered by the BOW83 catalog.

by taking galaxies from the deeper BOW83 catalog, which is complete up to $f_{57} \sim 22$. This resulted in much more features in the density maps than above, due to the introduction of the faint galaxy population of the clusters. The X-ray emission roughly follows the density contours of these maps. However, the apparent regularity of the X-ray isophotes may be due to the smoothing effect of the wavelet reconstruction, which favors larger scales against the smallest ones.

These figures show that the general structure of both clusters, A222 and A223, is extremely complex, presenting several clumps of galaxies in projection on their central regions, the reality of which is hard to assert in the absence of much more radial velocity data than that provided in this paper. Moreover, the fact that this complexity is not seen in the brighter DSS projected density, indicates that the projected clumps are mainly populated by faint galaxies. The X-ray emission is centered, for both clusters, in their main galaxy concentrations, but this does not correspond to location of their brightest members, as it is usually observed in nearby rich clusters of galaxies. All these pieces of data support the view that we are facing a dynamically unrelaxed, young system.

For the more X-ray luminous cluster A223 (Figure 3b), we notice the presence of an extended emission at North, centered near the position of the brightest galaxy of the

Table 1. Heliocentric redshifts for galaxies.

GALAXY	R.A. (2000)	DEC. (2000)	f_{57} mag	$j - f_{57}$ mag	HEL. VEL. $V \pm \Delta V$	TDR value	N
A222							
01 37 10.00	-12 59 56.7				63395 123	2.56	c
01 37 14.54	-12 59 20.4				64999 76	4.13	c
01 37 19.75	-13 00 42.3	18.81	1.66		64982 77	5.70	c
01 37 21.32	-13 00 39.9	18.40	1.68		66371 64	4.26	c
01 37 21.34	-12 59 22.9	19.99	1.62		63628 70	4.79	e
01 37 22.05	-12 58 59.9	20.71	1.17		62646 68	2.85	e
01 37 22.72	-13 00 23.0	18.33	1.61		63441 82	5.31	c
01 37 24.57	-12 57 50.8	20.98	0.90		82493 85	2.32	e
01 37 25.22	-13 00 21.7	20.80	1.49		66352 68	2.91	e
01 37 25.35	-12 59 50.8	19.47	1.29		51476 43	3.33	c
01 37 26.45	-12 59 58.5	17.91	1.83		64024 21	6.16	c
01 37 28.02	-13 00 03.0	19.71	1.60		64178 40	9.97	e
01 37 28.96	-12 59 26.4	19.09	0.94		54700 ??		c
					54863 30		l
01 37 29.53	-12 59 50.2	19.73	1.51		65510 104	3.62	e
01 37 29.70	-13 00 26.8	20.29	1.69		63869 110	3.46	c
01 37 30.88	-12 59 25.2	19.38	1.69		64859 20	10.42	e
					64957 25	5.48	c
					64847 210		l
01 37 31.64	-12 58 52.4	19.52	1.69		65025 33	8.18	e
01 37 32.63	-12 58 43.7	20.56	1.41		65274 74	4.98	e
01 37 32.74	-12 59 19.0	20.35	1.62		64148 70	3.18	c
01 37 33.50	-12 59 00.0	20.17	1.56		64448 28	9.46	e
01 37 33.49	-12 59 28.0	18.69	1.63		65057 500		s
01 37 34.13	-12 59 30.1	17.87	1.83		64115 37	6.59	c
01 37 34.48	-12 59 46.3	18.98	1.79		65895 65	3.96	c
01 37 34.54	-12 59 24.0	19.56	1.66		63857 90		l
01 37 34.61	-12 58 41.1	19.13	1.68		62911 33	10.14	e
01 37 35.59	-12 59 26.8	19.01	1.46		62974 46	5.28	c
					62748 150		l
01 37 37.24	-12 59 16.0	19.32	0.82		64277 60		l
01 37 38.67	-12 59 24.4	20.49	1.55		62504 122	2.30	c
01 37 40.06	-12 58 31.0	19.16	1.15		63887 180		l
01 37 40.18	-12 59 56.6	19.92	1.62		63430 54	3.52	c
01 37 41.59	-12 58 31.9	17.98	1.72		64181 67	3.68	c
01 37 42.60	-13 00 37.7	19.69	1.59		64370 112	3.62	c1
01 37 43.00	-12 57 44.0	18.31	1.82		64067 30		l
A223							
01 37 32.31	-12 52 43.7				z=0.3063		c2
01 37 35.38	-12 49 57.3				62304 22	6.53	c
01 37 36.08	-12 53 42.6				62461 71	3.87	c
01 37 40.75	-12 52 00.9				63782 72	5.46	c
01 37 41.62	-12 52 15.4				62387 72	4.54	c
01 37 44.02	-12 51 10.1	19.83	0.93		82918 36		c3
01 37 44.84	-12 50 57.3	19.47	1.79		83377 40	6.20	c
01 37 44.86	-12 44 48.5	19.91	1.73		82227 43	5.05	c
01 37 45.48	-12 46 27.1	19.04	1.47		61485		c4
01 37 46.01	-12 49 49.4	19.34	1.57		83432 57	5.23	c
01 37 49.59	-12 51 37.6	18.88	1.63		64595 50	7.46	c
01 37 50.82	-12 51 01.1	19.75	1.60		63738 98	3.88	c
01 37 51.16	-12 47 33.7	19.31	0.67		z=0.4726		c5
01 37 52.14	-12 47 41.4	18.98	1.56		65350 89	3.61	c

GALAXY	R.A. (2000)	DEC. (2000)	f_{57} mag	$j - f_{57}$ mag	HEL. VEL. $V \pm \Delta V$	TDR	N
	01 37 52.23	-12 49 54.0	19.48	1.58	64440 98	5.18	c
	01 37 53.04	-12 50 15.3	19.41	1.63	star		c
	01 37 54.96	-12 49 55.0	19.43	1.57	63273 79	4.22	c6
	01 37 55.35	-12 51 31.1	19.39	1.57	63200 41	5.47	c
	01 37 56.07	-12 49 11.7	18.33	1.68	63716 89	2.96	c
	01 37 56.12	-12 48 17.0	18.37	1.68	62778 120		l
	01 37 56.89	-12 49 12.6	19.12	1.58	62341		c7
	01 37 57.28	-12 50 18.9	18.20	1.33	62473 11		c8
					62208 90		l
	01 37 57.18	-12 48 51.0	18.66	0.87	62358 500		s
	01 37 57.48	-12 47 57.0	18.44	1.71	62868 120		l
	01 37 58.14	-12 50 55.5	19.31	0.99	63966 89	3.26	c
	01 37 58.24	-12 49 22.0	18.58	1.35	41732 90		l
	01 37 59.90	-12 47 34.6	20.56	1.33	64192 98	2.57	c
	01 38 02.40	-12 45 21.7	17.63	0.00	61532 39	3.43	c
					61476 92	2.45	p
					61758 500		s
	01 38 04.12	-12 44 50.4	17.73	0.00	15209 47	3.81	p
A520							
	04 54 01.23	+02 57 46.0	17.00	1.99	62172 37	4.71	c
	04 54 05.12	+02 53 30.0	17.72	1.22	60859 500		s
	04 54 05.63	+02 57 01.7	18.30	0.94	61145 75	3.51	c
	04 54 05.98	+02 55 55.4	19.47	1.97	60032 60	3.72	c
	04 54 07.24	+02 57 48.4	19.60	1.16	66926 65		c9
	04 54 07.92	+02 57 03.3	19.84	2.17	67830 78	2.93	c
	04 54 09.51	+02 58 18.1	19.34	1.89	59498 63	2.45	c
	04 54 12.01	+02 58 07.8	17.55	2.03	62256 35	6.32	c
	04 54 13.14	+02 57 33.8	17.17	1.96	60115 16	4.96	c
	04 54 14.10	+02 57 09.9	17.27	2.04	59506 46	4.87	c
					59420 60		l
	04 54 15.18	+02 57 08.2	17.89	1.96	59224 92	4.52	c
	04 54 16.14	+02 56 42.7	17.87	2.01	58808 87	3.14	c
	04 54 17.33	+02 56 46.1	20.22	1.91	64056 81	3.07	c
	04 54 19.27	+02 58 26.3	18.46	1.93	60941 96	2.28	c
	04 54 19.94	+02 57 44.6	17.02	2.03	60381 53	3.91	c
	04 54 20.30	+02 55 37.0	17.08	1.94	58581 60		l
	04 54 20.72	+02 55 29.5	17.89	1.98	58482 97	2.34	c
	04 54 21.41	+02 56 47.6	18.96	2.04	60118 80	2.67	c
	04 54 22.24	+02 55 07.0	18.88	2.06	59150 300		l
	04 54 23.23	+02 56 40.8	18.86	1.95	73474 83	2.53	c
	04 54 25.00	+02 58 57.5	19.04	1.43	60370 71	3.47	c
	04 54 25.52	+02 59 37.5	20.85	1.84	60315 98	2.21	c
	04 54 27.87	+02 55 28.4	19.25	2.39	62563 91	2.86	c
	04 54 28.95	+02 56 46.6			69839 98	2.34	c
	04 54 31.46	+02 57 24.7			z= 0.373		c10
	04 54 32.74	+02 54 48.3			60862 49	5.36	c
	04 54 34.68	+02 56 50.6			58629 57	2.56	c
					z= 0.334		c11

Notes. **1:** $H\beta = 64420 \text{ km s}^{-1}$; **2:** measured on [OII], $H\beta$, [OIII] and $H\alpha$; **3:** measured on the strong $H\alpha$; **4:** measured on the strong $H\beta$; **5:** measured on [OII]; **6:** $H\beta : 63329 \text{ km s}^{-1}$; **7** and **8:** measured on [OII], $H\beta$ and [OIII]; **9:** measured on $H\alpha$; **10:** measured on H and K lines; **11:** second object on the line of sight.

cluster (the Northeast one). This emission is almost coincident with a projected substructure of galaxies delineated by the isopleth curves, suggesting that this is a real feature of the cluster.

We have used the ROSTAT statistical package (Beers et al. 1990; see also Ribeiro et al. 1998 and references therein) to analyze the velocity distributions obtained in this paper. ROSTAT provides several robust estimators for the location, scale and shape of one-dimensional data

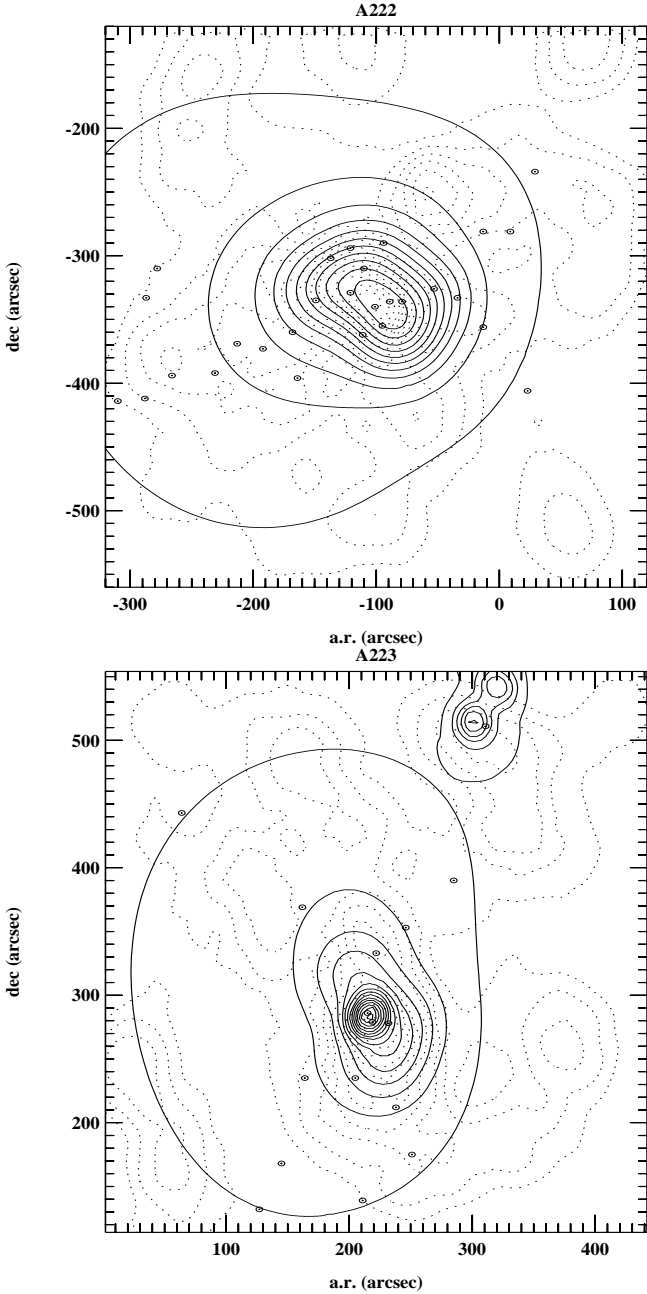


Fig. 3. a. X-ray isophotes from the ROSAT/HRI image of A222. A mean background has been subtracted from the original image which was then reconstructed using wavelet transform and excluding the smallest scales, due to intrinsic photon noise. The dashed lines give the significance map of the galaxy projected densities from the BOW83 catalog (only the highest density levels are displayed). Other symbols have the same meaning as for Figure 2. b. Like Figure 3a but for A223.

sets. It includes a variety of normality tests as well as a conservative unimodality test of the distribution (the Dip test, see Hartigan & Hartigan 1985). The shape estimators given by ROSTAT are the Tail Index (TI) and the Asym-

metry Index (AI) (for a thorough discussion on these two indexes, see Bird & Beers 1993). Since we will be dealing with poor samples, we have restricted ourselves to the use of the so called biweighted estimators of location and scale (see Beers et al. 1990 for a definition), which generally perform better in these cases. We notice, however, that the values of the biweighted estimators obtained here differ negligibly from that obtained using other commonly used estimators such as the conventional mean and dispersion obtained from recursive 3σ -clipping (Yahil & Vidal, 1977), or median estimators.

Our radial velocity sample for the A222 and A223 system consists of 53 spectroscopically measured galaxies to which we added another 9 taken from the literature (see Table 1). Although by no means complete, this sample is spatially reasonably well distributed to allow us some preliminary analysis. Figure 4 shows the corresponding wedge velocity diagram in right ascension and declination for A222 and A223.

After removing some obvious background and foreground galaxies – also confirmed by the recursive 3σ clipping – we obtained a sample of 50 galaxies with measured velocities corresponding to the main peak seen in the inset of the upper panel of Figure 5, which displays the radial velocity distribution for the whole observed sample. The normality tests provided by the ROSTAT package fail to reject a Gaussian parent population for this sample. However, the Dip statistics has a value of 0.067, which is enough to reject the null hypothesis of unimodality at significance levels better than 10%. This is understandable, for this sample refers to both components of the binary system A222 and A223. Its mean velocity is $V_{bi} = 63833 \pm 165 \text{ km s}^{-1}$, with dispersion $\sigma_{bi} = 1157 \pm 119 \text{ km s}^{-1}$. This places the system at redshift $z = 0.21292$, slightly higher than the value quoted by Struble & Rood (1987).

The lower panels of Figure 5 display the separate velocity distribution for the southern subsample (30 galaxies), which corresponds to A222, and for the northern one (20 galaxies), corresponding to A223 (see Figure 2). The normality tests do not reject Gaussian parent populations for any of these subsamples. The A222 galaxies have slightly higher velocities than those of A223: mean velocities are $V_{bi} = 64242 \pm 194 \text{ km s}^{-1}$, for A222, and $V_{bi} = 63197 \pm 266 \text{ km s}^{-1}$ for A223. However, if we remove 4 galaxies belonging to the bridge connecting the two clusters (see Figure 2), the mean velocity of A223 increases to $V_{bi} = 63348 \pm 295 \text{ km s}^{-1}$, slightly reducing the significance of the velocities difference. Note that 3 of these galaxies locate at the low velocity tail of A223, as displayed in Figure 5. The velocity dispersion of the two clusters are about the same: $\sigma_{bi} = 1013 \pm 150 \text{ km s}^{-1}$ for A222 and $\sigma_{bi} = 1058 \pm 160 \text{ km s}^{-1}$ for A223 (1123 ± 191 when the bridge galaxies are removed).

Table 2 gives mass and mass-luminosities ratio estimates for each cluster separately, obtained with the virial

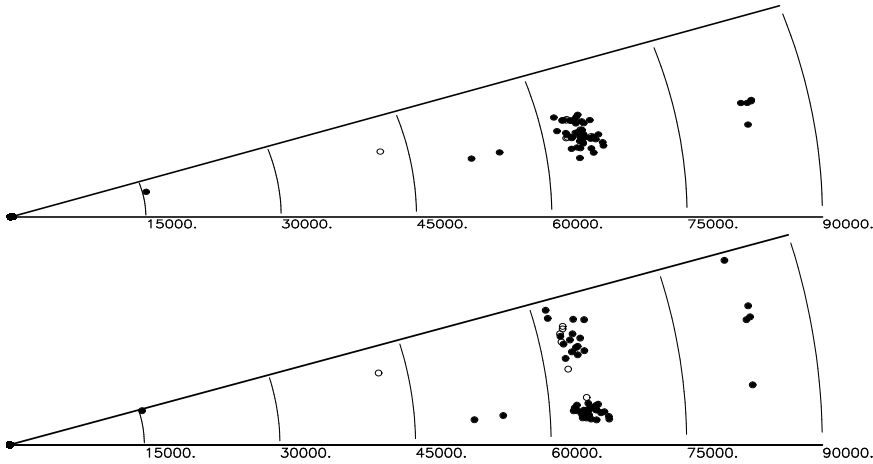


Fig. 4. Wedge velocity diagram in right ascension (up), and declination (down) for the measured galaxies in A222 and A223. Filled symbols represent galaxies measured in the present work; open symbols represent galaxies with velocities from the literature.

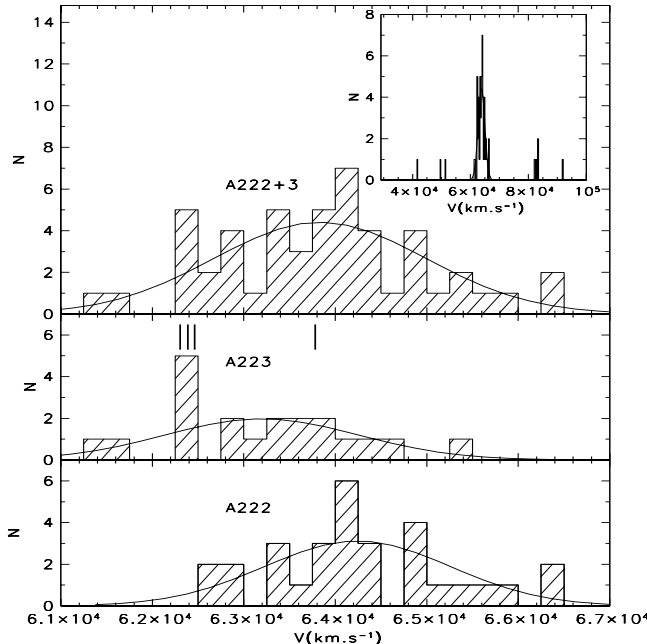


Fig. 5. The radial velocity distribution for the southern (lower panel) and northern (middle panel) subsamples of galaxies. The vertical lines in the middle panel display the velocities of the 4 galaxies belonging to bridge connecting the two main concentrations. The upper panel shows the velocity distribution of the sample of both clusters taken together. The continuous lines display Gaussians curves with means and dispersions values as given in the text. The inset shows the velocity distribution for the whole sample of measured galaxies.

and projected mass estimators given by Heisler et al. (1985), for the case where all the cluster mass is supposed to be contained in the galaxies, and by Bahcall & Tremaine (1981), under the hypothesis that galaxies are

test particles orbiting in a dark mass spherical potential. Total j luminosities were estimated from the BOW83 catalog, which is complete up to $j = 22$.

3.2. The cluster A520

The analysis of A520 data proceeded in the same lines as that of the A222+A223 system. Figure 6 displays the significance map of projected densities of the DSS galaxies in the field of A520. This figure also displays the positions of 21 galaxies having measured radial velocities and belonging to the cluster, as discussed below. As for the case of A222/3, here also we can see that the main concentration has two extensions, possibly due to infalling clumps of galaxies.

In Figure 7 we display the X-ray isophotes of a wavelet reconstruction of the ROSAT/HRI image of A520, superposed to the significance map of the projected density of galaxies (dashed lines). As before, this map was constructed by taken galaxies from the BOW83 catalog, showing that the cluster may be much more complex than it could be noticed from the DSS map, although the reality of the substructures shown here cannot be assigned in view of the paucity of radial velocity data.

As it can be seen from this figure, although the main X-ray emission roughly follows the projected density of galaxies, it seems dislocated relatively to main concentration of A520, located near the center of this field. The peak X-ray emissivity comes from a very compact region which may be consistent with a point-like source, almost coincident with a “blue” galaxy ($j - f_{57} = 1.22$), originally assigned by Sandage, Kristian & Westphal (1976) as one of the brightest A520 members (it ranks a 7th place in j magnitudes but only 19th in f_{57} magnitudes). In fact, as displayed in Figure 7, the f_{57} brightest members of A520 do not seem to belong to any of the main galactic

Table 2. Mass and M/L estimates

(1) Cluster	(2) R	(3) L_j	(4) N_L	(5) N_v	(6) Mass		(7) M/L		(8) Notes
					Virial	Proj.	Virial	Proj.	
A222	200"	1.15	107	27	7.55 ± 2.56	10.05 ± 3.39	658	876	a
					2.85	5.22 ± 1.29	248	450	b
A223	350"	1.46	140	30	8.08 ± 2.60	10.25 ± 3.27	553	701	a
					2.91	5.30 ± 1.24	199	363	b
A520	200"	1.13	84	10	6.69 ± 3.73	12.69 ± 7.02	686	11230	a
					3.84	7.05 ± 2.97	340	624	b
A520	350"	1.49	124	16	10.17 ± 4.47	19.62 ± 8.58	684	13190	a
					5.50	10.46 ± 3.41	370	731	b
A520	200"	2.57	166	16	12.33 ± 5.42	16.74 ± 7.33	481	625	a
					6.71	8.93 ± 2.91	261	348	b
	350"	3.78	234	20	15.73 ± 6.19	20.91 ± 8.18	428	569	a
					8.01	11.01 ± 3.19	218	300	b

column(1): Cluster Name, column(2): radius in arcsec., column(3): total luminosity with $j < 22$ in $10^{12}h_{50}^{-2}L_\odot$, column(4): number of galaxies with $j < 22$, column(5): number of galaxies with measured velocity, column(6): mass of the cluster in $10^{14}h_{50}^{-1}M_\odot$, column(7): mass-luminosity ratio in solar units, column(8): mass estimators: (a) self-gravitating system, (b) test particle system.

clumps observed, a situation which is similar to that already noticed in the case of A222. This means that most of the clumps are constituted by the faint galaxy population, not present in the DSS sample. We may conclude that, unless we are facing a serious case of background contamination, the A520 cluster, as for A222, may be an example of a dynamically young system where clumps of galaxies are still in phase of collapsing on its dark matter gravitational well, probably located at the mean center of the X-ray emission region seen in Figure 7. Unfortunately there is no X-ray spectra available for A520 (as also for A222/3), what hinders a more detailed diagnostic of the evolutive dynamical stage of the cluster.

Our sample of spectroscopically measured objects in the field of A520 (Table 1) has 28 galaxies, with 25 coming from the observations reported here and 3 others from the literature (Sandage, Kristian & Westphal 1976; Newberry, Kirshner & Boroson 1987).

Figure 8 shows the wedge velocity diagram in right ascension and declination for A520.

The 3σ clipping of the total radial velocity distribution leaves 21 galaxies kinematically linked to the cluster. This sample is consistent with normality under all the statistical tests included in the ROSTAT routine. For comparison, we applied the same tests to a sample including the

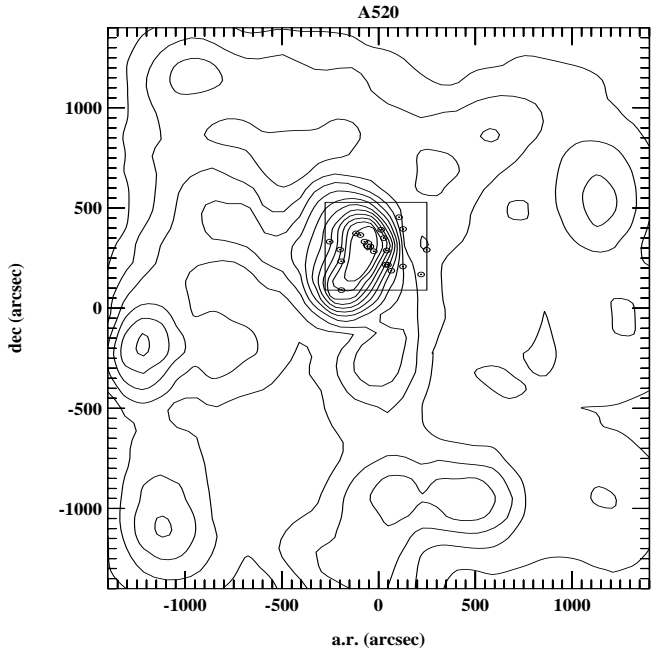


Fig. 6. Projected density map (*significance map*) of the galaxies in the field of A520 (centered at $\alpha_{2000} = 04^h54^m18^s$, $\delta_{2000} = +02^\circ52'00''$). The symbols have the same meaning as in Figure 2.

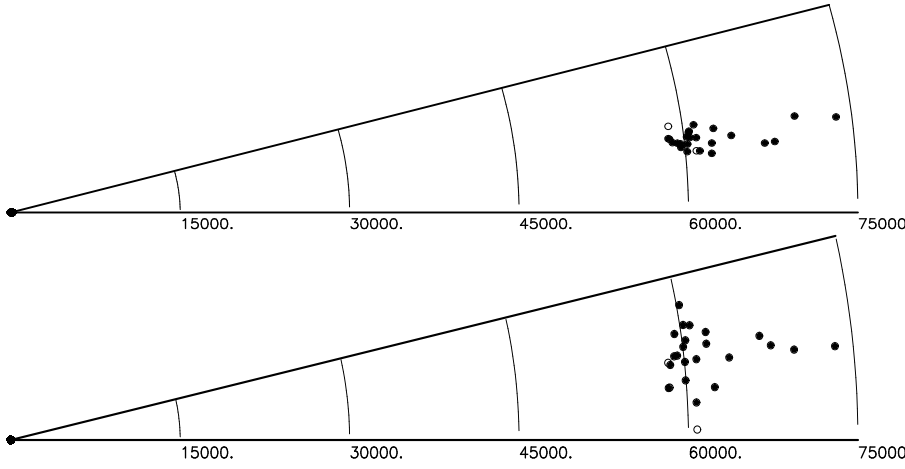


Fig. 8. Wedge velocity diagram in right ascension (up), and declination (down) for the measured galaxies in A520. Filled symbols represent galaxies measured in the present work; open symbols represent galaxies with velocities from the literature.

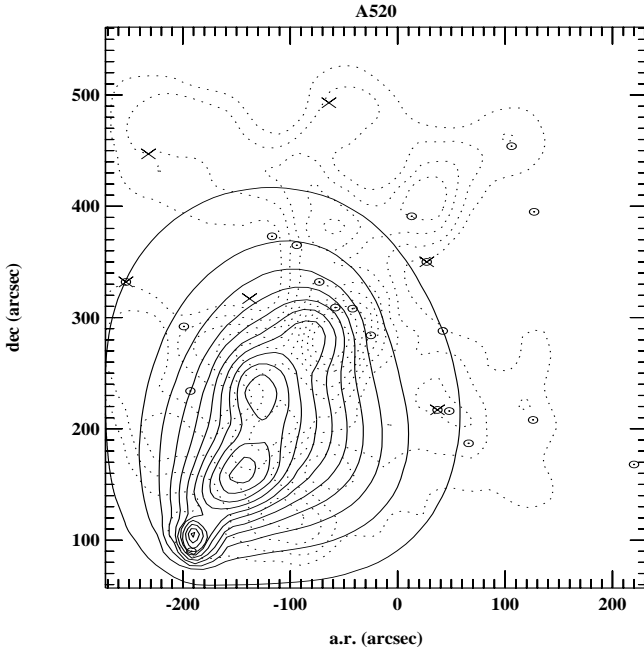


Fig. 7. Like Figure 3a but for A520. The 6 brightest members of the cluster are marked with crosses.

less discrepant galaxy, in velocity space, excluded by the 3σ clipping. Although the tests fail to reject the normality for this sample, it resulted skewed towards higher velocities, as indicated by the Asymmetry Index obtained: $AI = 0.85$.

Figure 9 displays the velocity distribution of the 21 retained galaxies as well as that of the whole sample (inset). The mean velocity for this sample is $V_{bi} = 60127 \pm 284$ km s $^{-1}$, with dispersion $\sigma_{bi} = 1250 \pm 189$ km s $^{-1}$, placing the cluster at redshift $z = 0.20056$. The values for the mass and mass-luminosity ratio, calculated under the

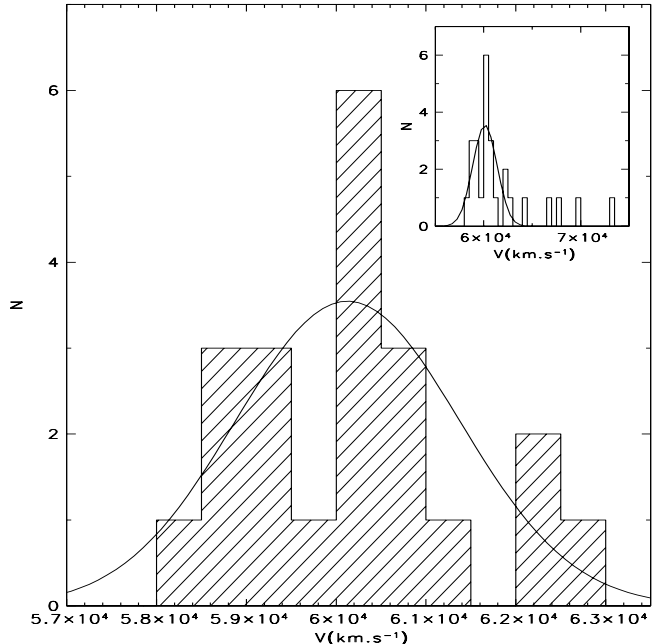


Fig. 9. The radial velocity distribution for the A520 sample of galaxies. The continuous curve shows the Gaussian distribution corresponding to the mean velocity and dispersion quoted in the text (normalized to the sample size and range). The inset shows the velocity distribution for the whole sample of measured galaxies.

same hypothesis as for A222 and A223, are given in Table 2.

4. Spectral Classification

Spectral classification has been performed through a Principal Component Analysis (PCA) of the spectra. This technique makes use of all information contained in the spectra (except in the emission lines; see below) and, in

this sense, it can provide a classification scheme more powerful than those based on the amplitude of individual absorption lines. Here we apply the method to a sample of 51 CFHT spectra of galaxies that are probably members of the clusters A222, A223 and A520 (section 3) to obtain spectral types. The point to be stressed is that the spectra of normal galaxies form a sequence- the spectral sequence- in the spectral space spanned by the M -dimensional vectors that contain the spectra, each vector being the flux of a galaxy (or a scaled version of it) sampled at M wavelengths (Sodré & Cuevas 1994, 1997; Connolly *et al.* 1995; Folkes *et al.* 1996). The spectral sequence correlates well with the Hubble morphological sequence, and we define the “spectral type” (hereafter ST) of a galaxy from its position along the spectral sequence. Following Sodré & Cuevas (1997), we associate the spectral type ST of a galaxy with its value for the first principal component. Note that, since we are working with uncalibrated spectra, only a relative classification is possible, that is, we are only able to know whether a galaxy has an earlier or later spectral type than the others in the sequence (Cuevas, Sodré & Quintana 2000).

We have jointly analyzed the spectra of galaxies in the three clusters because the differences in their redshifts are small and the observed spectra sample essentially the same rest-frame wavelength interval. PCA was applied to a pre-processed version of 51 CFHT uncalibrated galaxy spectra (33 were spectra of galaxies of A222 and A223 and 18 of A520). Firstly, the spectra were shifted to the rest frame and re-sampled in the wavelength interval from 3440 Å to 5730 Å, in equal-width bins of 2 Å. Secondly, we removed from the analysis 8 regions of ~ 40 Å each centered at the wavelengths of [OII] $\lambda 3727$, NeIII $\lambda 3869$, H δ $\lambda 4102$, H γ $\lambda 4340$, HeII $\lambda 4686$, H β $\lambda 4861$, [OIII] $\lambda 4959$ and [OIII] $\lambda 5007$. This was done in order to avoid the inclusion of emission lines in the analysis, which increases the dispersion of the spectra in the principal plane (mainly due to an increase in the second principal component). The spectra, now sampled at $M = 980$ wavelength intervals, were then normalized to the same mean flux ($\sum_\lambda f_\lambda = 1$). Finally, we subtracted the mean spectrum from the spectrum of each galaxy and use the PCA to obtain the principal components. This procedure is equivalent to the conventional PCA on the covariance matrix (that is, the basis vectors are the eigenvectors of a covariance matrix).

Figure 10 shows the projection of the spectra of the 51 galaxies of the three clusters on to the plane defined by the first two principal components. They contain only 24% of the total variance, mainly due to the low signal-to-noise ratio of several spectra (the median S/N is ~ 5.8 in the interval between 4500 Å to 5000 Å). Indeed, in this figure different symbols correspond to different signal-to-noise intervals (see the figure caption), and the scatter in the second principal component seems to increase as the signal-to-noise ratio decreases. On the other side, numerical simulations indicate that the noise does not introduce

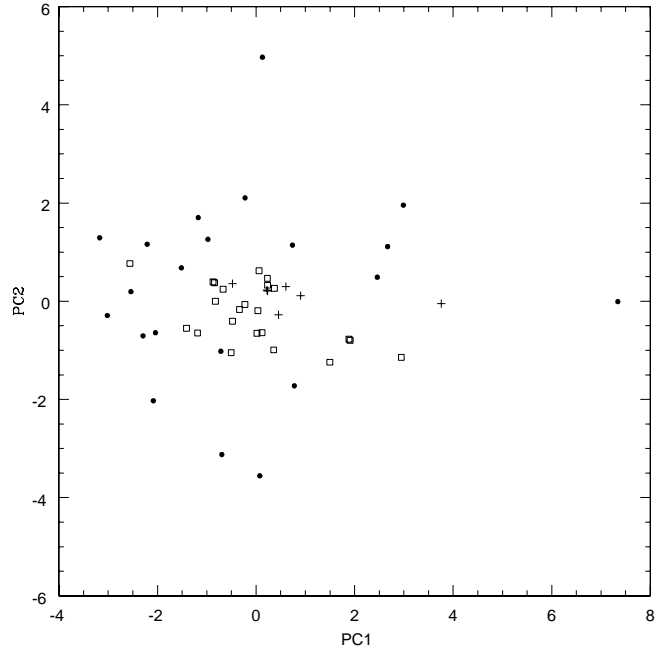


Fig. 10. Projection of the spectra of A222, A223 and A520 onto the first two principal components of the galaxies. Different symbols correspond to different signal-to-noise ratios, computed in the wavelength interval between 4500 Å and 5000 Å. Filled circles: $2.9 \leq S/N < 5.5$; squares: $5.5 \leq S/N < 8.0$; crosses: $S/N \geq 8.0$.

any significant bias in the spectral classification (Sodré & Cuevas 1997). Note that, in this figure, early-type galaxies are at the left side, and increasing values of ST (or, equivalently of the first principal component) correspond to later-type galaxies.

The low variance accounted for by the two first principal components may rise doubts about whether we are indeed measuring meaningful spectral types through the first principal component. A possible approach is to compare our classification with the spectral classification present in Newberry, Kirshner & Boroson (1988). These authors classified a few galaxies in A222, A223, and A520 in red or blue accordingly to their colors and position in a color-magnitude diagram, or from the strength of some absorption features present in the spectra. Unfortunately we have only four cluster galaxies in common with Newberry, Kirshner & Boroson (1988). Nevertheless our results are encouraging, because the three galaxies classified as red by Newberry, Kirshner & Boroson (1988) have spectral types equal to or smaller than ~ 1.5 , while the only galaxy classified as blue by them has a spectral type of 2.46. Additionally, as we will show, with these spectral types we are able to recover both the morphological and kinematical segregations for the galaxies in these clusters, indicating that our spectral types are indeed carrying useful morphological information.

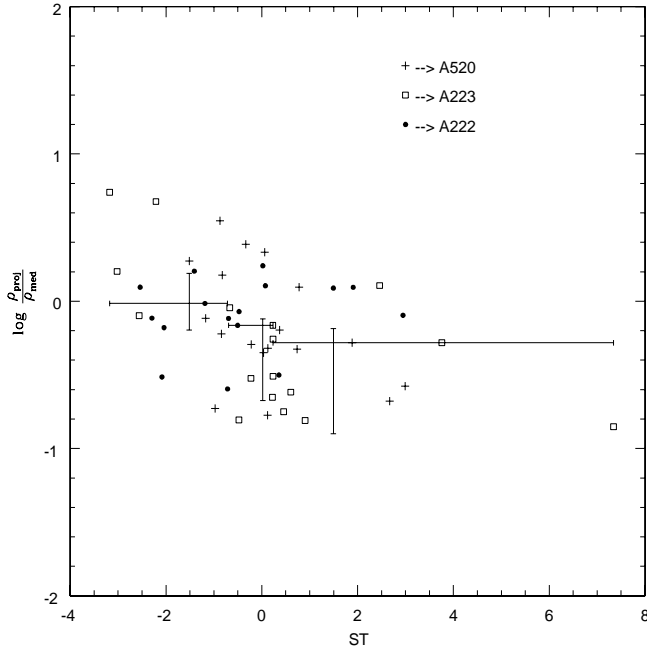


Fig. 11. Projected local density normalized by the median density of each cluster versus the spectral type. The points with error bars are the median values taken in bins of equal galaxy number. The vertical error bars correspond to the quartiles of the distribution, whereas the horizontal error bars indicate the interval of ST associated to each bin. Different symbols correspond to data of different clusters.

It is worth emphasizing that we base our spectral classification only on the properties of the stellar populations that are contained in the continuum and absorption lines, and that the emission lines enter in no way in the classification scheme. It is important to point out, however, that the emission lines of normal galaxies do correlate with spectral types; see Sodré & Stasińska (1999) for a detailed discussion of this subject.

5. Morphological and Kinematical Segregation

Now we use the spectral types of the galaxies to study whether the morphology-density relation (Dressler 1980) is present in these clusters. We have computed the projected local density from the 6 nearest (projected) neighbors of each of the galaxies in our spectroscopic sample with the estimator (Casertano & Hut 1985):

$$\rho_{proj} = \frac{5}{\pi r_6^2}$$

where r_6 is the projected distance of the 6th nearest galaxy. We have used the catalogue obtained from DSS (see section 3) to estimate the local density. Figure 11 shows the logarithm of the projected local density normalized by the median density of each cluster versus the spectral type.

This figure shows that, for A222, A223 and A520, early-type galaxies tend to be located in denser regions than late-type galaxies, indicating that the morphology-density relation (Dressler 1980), as inferred using spectral types, was already established in clusters at $z \sim 0.2$. The correlation shown in Figure 11 is significant: the Spearman rank-order correlation coefficient is $r_s = -0.41$ and the two-sided significance level of its deviation from zero is $p = 0.002$.

Nearby clusters also present a “kinematical segregation”: the velocity dispersion of early-type galaxies is lower than those of late-type galaxies (Sodré et al. 1989). This may be an evidence that late-type galaxies have arrived recently in the cluster and are not yet virialized, while the early-type galaxies constitute a relaxed systems with a low velocity dispersion. We present in Figure 12, as a function of spectral type, the absolute value of galaxy velocities relative to the clusters mean velocity, normalized by the velocity dispersion of each cluster. The points with error bars in this figure are the median values taken in bins of equal galaxy number; the vertical error bars correspond to the quartiles of the distribution, while the horizontal ones indicate the interval of ST corresponding to each bin. The data in Figure 12 indicate that early-type galaxies tend to have lower relative velocities than galaxies of later types; the Spearman rank-order correlation coefficient r_s is now 0.39 and the two-sided significance level of its deviation from zero is 0.005. Hence, these clusters seem to present the same kind of kinematical segregation detected in low redshift galaxy clusters.

6. Summary

We have presented here an analysis of three medium redshift clusters, A222, A223, and A520, based on new observations of radial velocities in the field of these clusters. Through observations made at the Canada-France-Hawaii Telescope, the European Southern Observatory, and the Pic du Midi Observatory, we obtained a set of 78 new redshifts, 71 of them corresponding to galaxies members of these clusters.

From these observations and velocities and X-ray data from the literature we concluded that A222 and A223 have similar radial velocities and velocity dispersions, and will probably merge in the future, as already suggested by Sandage, Kristian & Westphal (1976). A520 also seems to be undergoing strong dynamical evolution, since its cD galaxy is not located at the center of the galaxy distribution (that is also coincident with the X-ray emission).

We have used spectra taken at CFHT to obtain, through a Principal Component Analysis, spectral types for a subset of 51 galaxies in these clusters. We have shown that galaxies of “early” spectral types tend to be found in regions with densities larger than that where “late” spectral type galaxies are found, suggesting that the morphology - density relation was already established at $z \sim 0.2$.

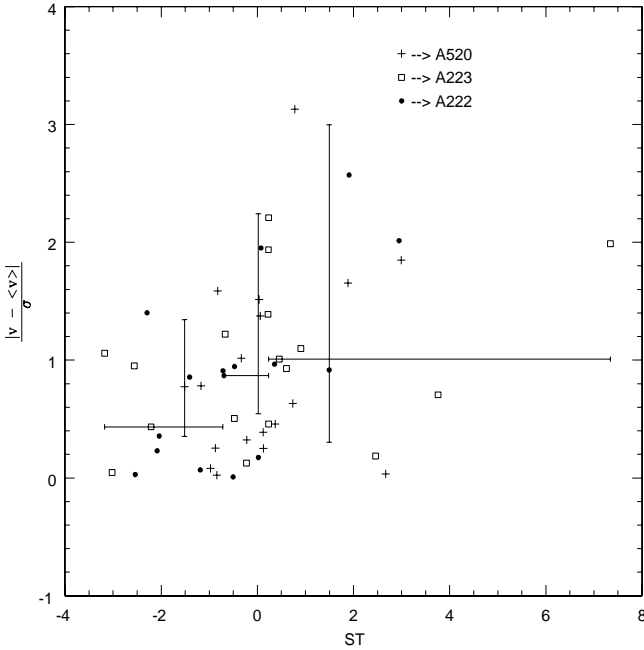


Fig. 12. Velocity corrected to the cluster mean velocity and normalized by the velocity dispersion of each system versus the spectral type. The three clusters are plotted together, with different symbols corresponding to different clusters. The errors bars have the same meaning as in Figure 11.

We have also found that galaxies with “early” spectral types tend to have lower velocity dispersions when compared with “late” spectral type galaxies, evidencing that the kinematical segregation too was already established at intermediate redshifts. These results are interesting because, despite the fact that these clusters are probably in a stage of strong evolution, they already show features that are expected for relaxed structures, as is the case of the segregations mentioned above.

Acknowledgements. We thank Christian Vanderriest for his collaboration in the CFHT observations and the CFHT, ESO and TBL staff. BTL, HC, HVC, and LSJ have benefited from the support provided by FAPESP, CNPq and PRONEX/FINEP to their work. We also thank an anonymous referee for useful comments that allowed us to improve the paper.

References

Bahcall J.N., Tremaine S., 1981, *ApJ*, 244, 805.
 Beers T.C., Flynn K., Gebhart K., 1990, *AJ*, 100, 32.
 Bertin E., Arnouts S., 1996, *A&AS*, 117, 393.
 Bird C.M., Beers T.C., 1993, *AJ*, 105, 1596.
 Biviano A., Durret F., Gerbal D., le Fevre O., Lobo C.,
 Mazure A., Slezak E., 1996, *A&A*, 311, 95.
 Bromley B.C., Press W.H., Lin H., Kirshner R.P., 1998,
ApJ, 505, 25.
 Butcher H., Oemler A., Wells D.C., 1983, *ApJS*, 52, 183
 (BOW83).
 Casertano S., Hut P., 1985, *ApJ*, 298, 80.
 Cole S., 1989, PhD Thesis.
 Connolly A.J., Szalay A.S., Bershady M.A., Kinney A.L.,
 Calzetti D., 1995, *AJ*, 110, 1071.
 Cuevas H., Sodré L., Quintana H., 2000, in preparation.
 Danese L., De Zotti G., di Tullio G., 1980, *A&A*, 82, 322.
 Dressler A., 1980, *ApJS*, 42, 565.
 Folkes S.R., Lahav O., Maddox S.J., 1996, *MNRAS*, 283,
 651.
 Galaz G., de Lapparent V., 1998, *A&A*, 332, 459.
 Hartigan J.A., Hartigan P.M., 1985, *Annals of Stat.*, 13,
 70.
 Heisler J., Tremaine S., Bahcall J.N., 1985, *ApJ*, 298, 8.
 Kurtz M.J., Mink D.J., Wyatt W.F., Fabricant D.G., Torres G., Kriss G.A., Tonry J.L., 1991, *ASP Conf. Ser.*, 25, 432.
 Lea S.M., Henry J.P., 1988, *ApJ*, 332, 81.
 Le Fèvre O., Crampton C., Lilly S.J., Hammer F., Tresse L., 1995, *ApJ*, 455, 60.
 Mink D.J., Wyatt W.F., 1995, *ASP Conf. Ser.*, 77, 496.
 Newberry M.V., Kirshner R.P., Boroson T.A., 1988, *ApJ*,
 335, 629.
 Ribeiro A.L.B., de Carvalho R.R., Capelato H.V., Zepf S.E., 1998, *ApJ*, 497, 72.
 Rué F., Bijaoui A., 1997, *Experim. Astron.*, 7, 129.
 Sandage A., Kristian J., Westphal J.A., 1976, *ApJ*, 205,
 688.
 Sodré L., Capelato H.V., Steiner J.E., Mazure A., 1989,
AJ, 97, 1279.
 Sodré L., Cuevas H., 1994, *Vistas in Astronomy*, 38, 287.
 Sodré L., Cuevas H., 1997, *MNRAS*, 287, 137.
 Sodré L., Stasińska G., 1999, *A&A*, 345, 391.
 Struble M.F., Rood H.J., 1987, *ApJS*, 63, 543.
 Tonry J., Davis M., 1979, *AJ*, 84, 1511.
 West M.J., Oemler A., Dekel A., 1989, *ApJ*, 346, 539.
 Yahil, A., Vidal, N.V., 1977, *ApJ*, 214, 347.